Supplementary information: Global strengthening of oceanic mesoscale currents over the satellite altimetry record

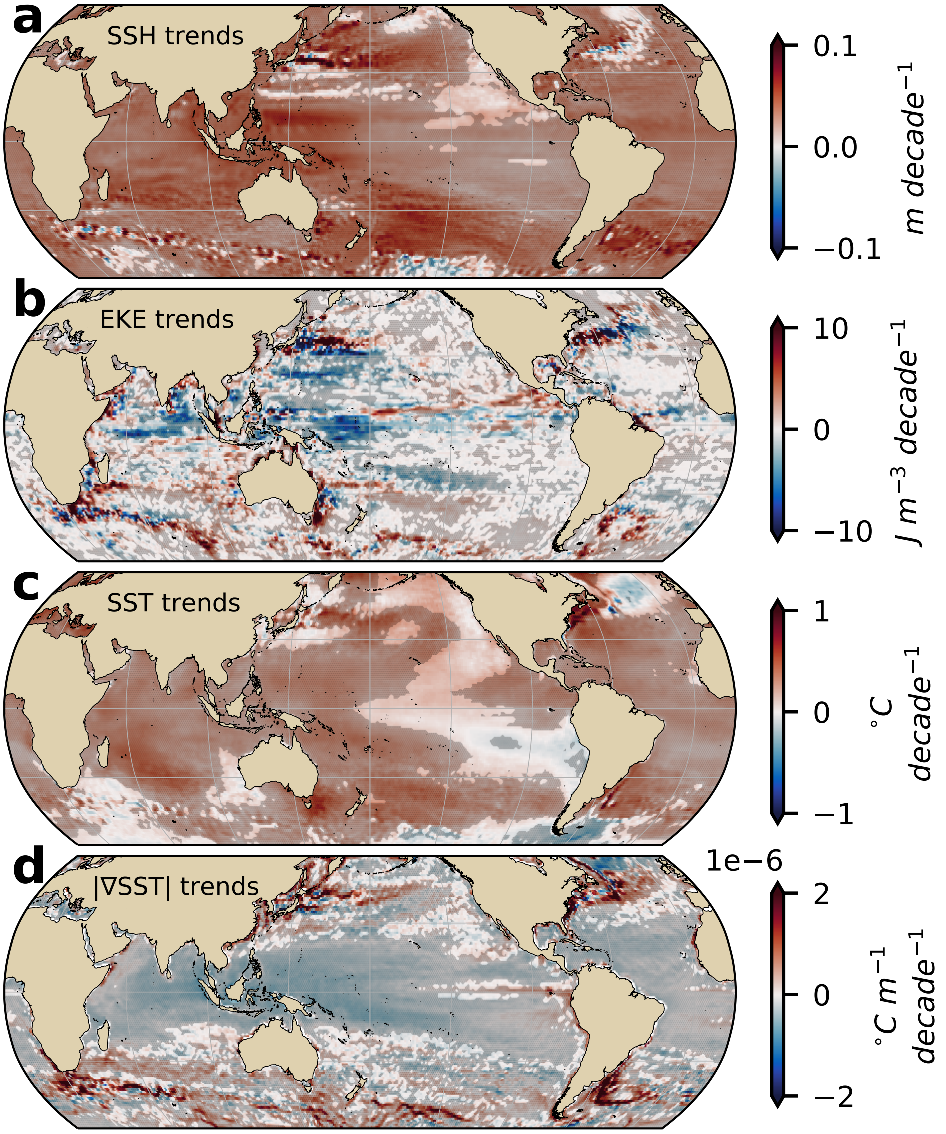

Figure S1 Regions of significant trends of (a) Sea Level Height; (b) Eddy Kinetic Energy; (c) Sea Surface Temperature; (d) Sea Surface Temperature Gradient. As per Fig.1, 2 in main manuscript, but showing in gray stippling regions that are significant above the 95% confidence level.

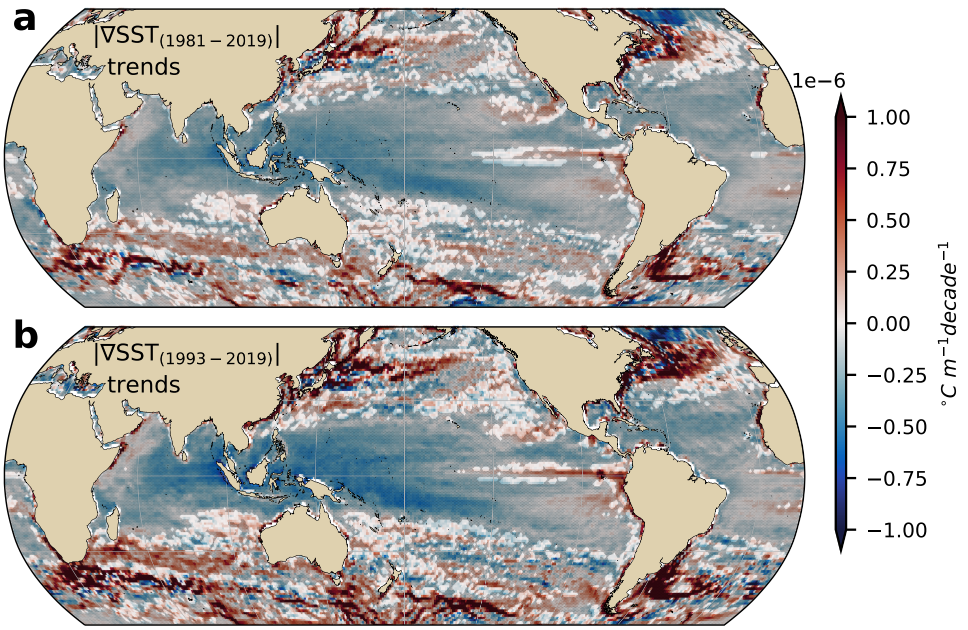

Figure S2 Sea Surface Temperature Gradient trends for periods between 1981-2019 and 1993-2019. Gray stippling shows regions that are significant above the 95% confidence level.

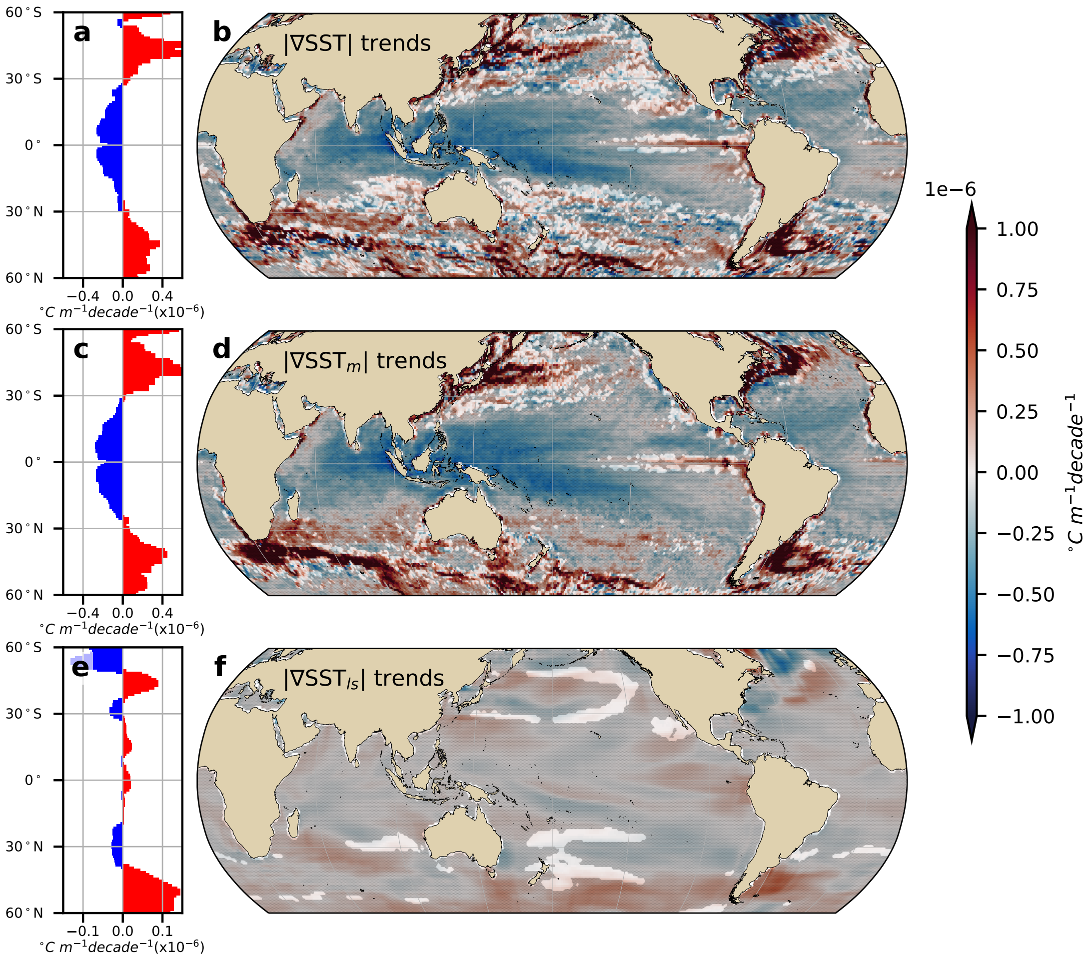

Figure S3 Sea Surface Temperature gradient trend scale analysis. Large-scale SST gradients are computed by filtering the SST field with a 3° kernel filter and a running average of 1 year before computing the gradients and their respective trends (See Methods). The small-scale correspond to the gradients of the SST minus the large-scale filtered SST field. (a) Zonally averaged SST gradient trends; (b) map of SST gradient trends; (c) zonally averaged small-scale SST gradient trends; (d) map of small-scale SST gradient trends; (e) zonally averaged large-scale SST gradients trend; (f) map of large-scale SST gradient trends. In panels (b), (d) and (f) gray stippling shows regions where the trends are significant above the 95% confidence level.

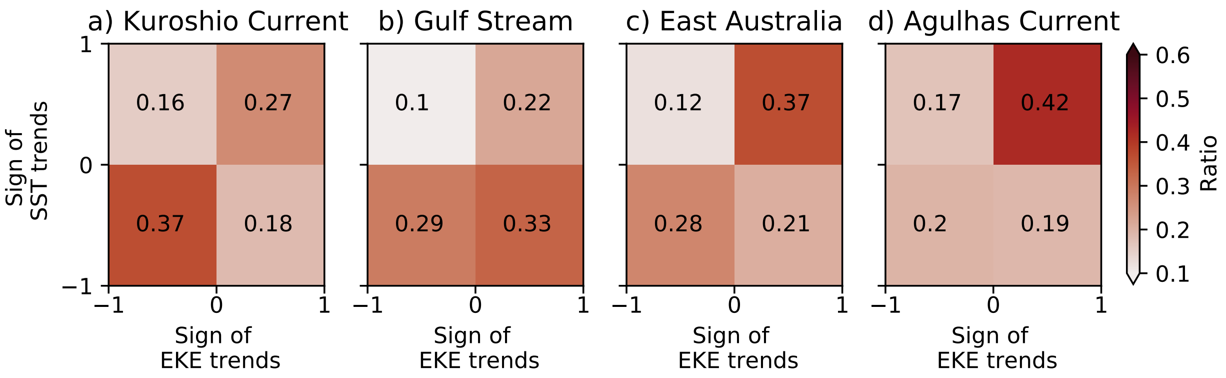

Figure S4 Regional ratio of mesoscale SST gradient trends and EKE trends signs. (a) Kuroshio current; (b) Gulf Stream; (c) East Australian current; (d) Agulhas retroflection. The ratio was computed by integrating the area weighted sign of the SST gradient trends and EKE trends divided by the total area of the region.

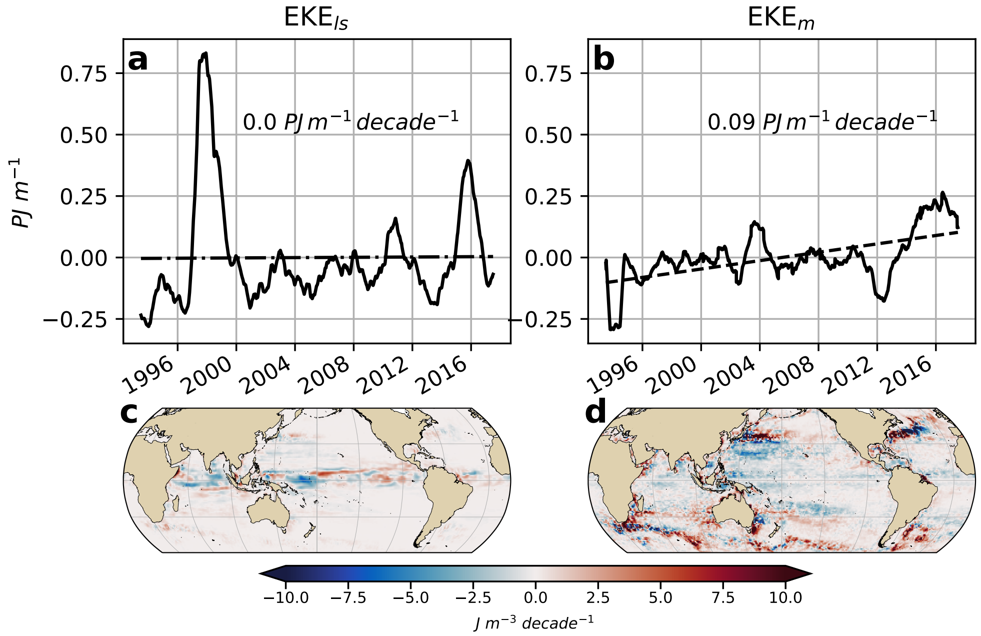

Figure S5 Eddy Kinetic Energy time series and trends computed from filtered velocities. Scales larger than typical mesoscale are computed by filtering the velocity fields with a 3° kernel filter (u_{ls}), and the smaller scales are calculated from the difference of the velocity fields and the filtered velocity field ($u_e = u - u_{ls}$). Then EKE and their respective trends are computed (See Methods). (a) EKE time series of scales larger than 3 degrees time series; (b) EKE time series of scales smaller than 3 degrees; (c) map of large-scale EKE trends; (d) map of small-scale EKE trends. Text in panels (a) and (b) correspond to trends per decade.

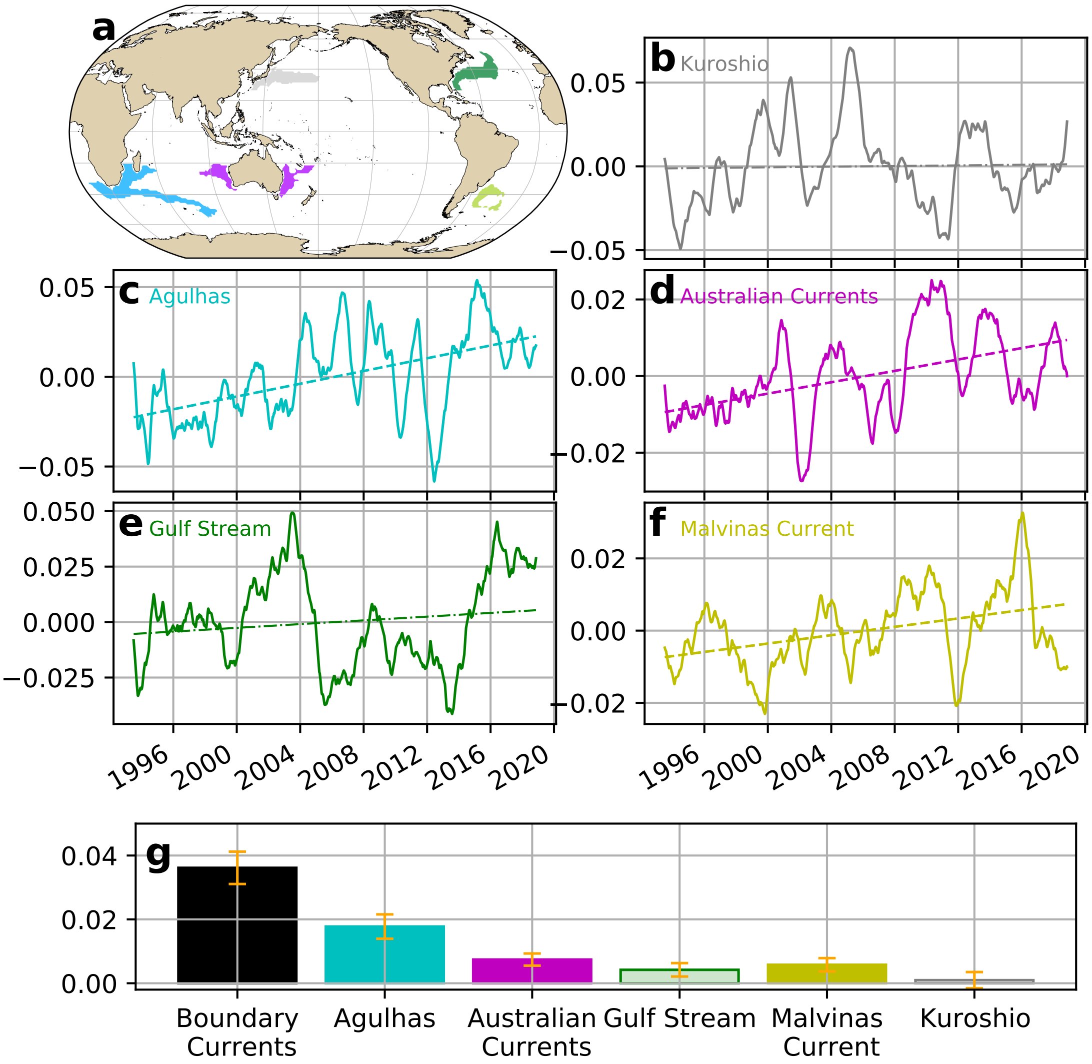

Figure S6 Time-series and trends of Eddy Kinetic Energy integrated over boundary currents. (a) Map of boundary current regions defined from climatological mean EKE and time series anomalies ($PJ\ m^{-1}$) and trends ($PJ\ m^{-1}\ decade^{-1}$) for each boundary current : (b) Kuroshio Current; (c) Agulhas Current; (d) East Australian Current and Leeuwin Current; (e) Gulf Stream; (f) Malvinas Current. (g) Linear EKE trends for boundary currents, uncertainties are shown in orange bars and statistically significant trends (above 95% confidence level) denoted with solid bars while non-significant trends are translucent.

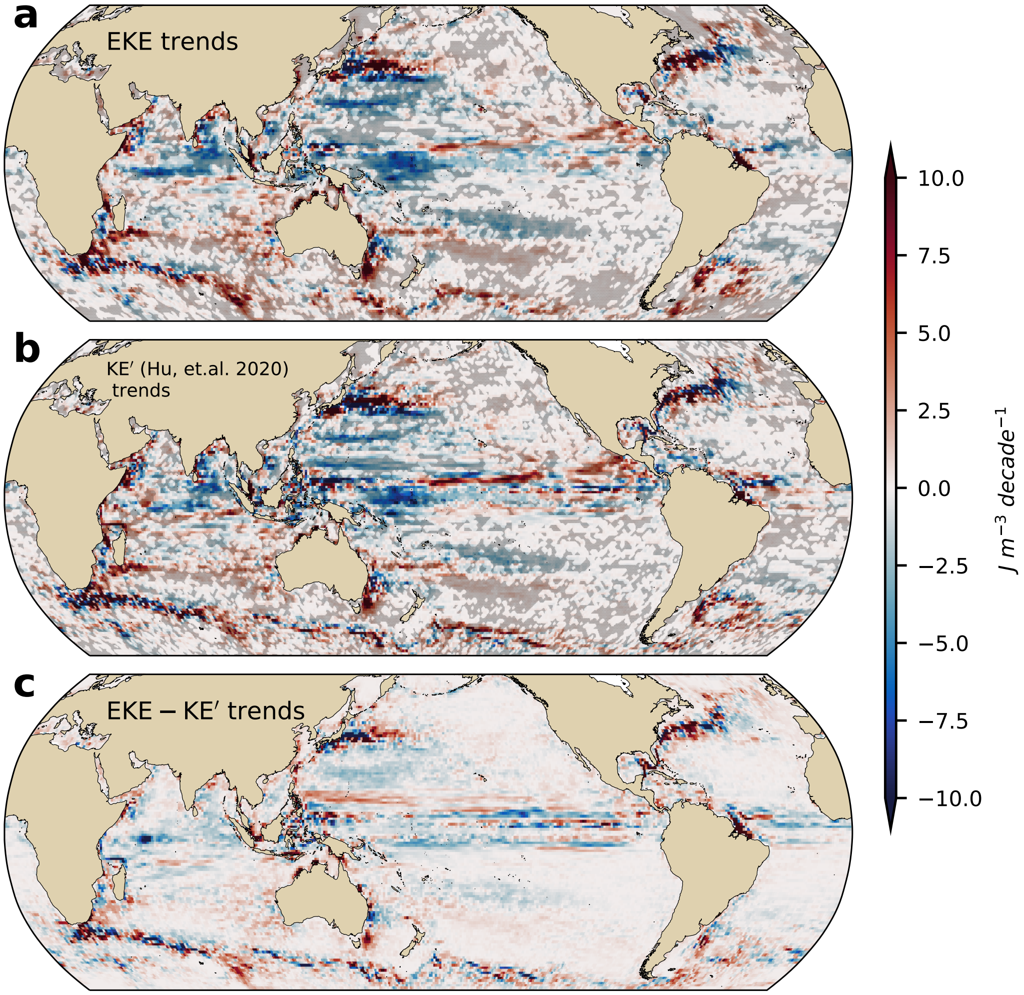

Figure S7 Comparison of satellite trends using EKE and Kinetic energy anomaly (KE') as computed by Hu et al. (a) EKE trend map, (b) KE′ trend map, and (c) difference between EKE and KE′ trends. The difference between the fields is a consequence of the cross terms due to the Reynolds velocity decomposition. In panel (a) and (b) gray stippling shows regions where the trends are significant above the 95% confidence level.